https://doi.org/10.5194/esurf-2020-50
Preprint. Discussion started: 8 July 2020

Earth Surface Dynamics Discussions

Relative terrestrial exposure ages inferred from meteoric ^{10}Be and NO_3^- concentrations in soils along the Shackleton Glacier, Antarctica

Melisa A. Diaz[1,2], Lee B. Corbett[3], Paul R. Bierman[3], Byron J. Adams[4], Diana H. Wall[5], Ian D. Hogg[6,7], Noah Fierer[8], W. Berry Lyons[1,2]

[1]School of Earth Sciences, The Ohio State University, Columbus, OH, 43210, USA
[2]Byrd Polar and Climate Research Center, The Ohio State University, Columbus, OH, 43210, USA
[3]Department of Geology, University of Vermont, Burlington, VT, 05405, USA
[4]Department of Biology, Evolutionary Ecology Laboratories, and Monte L. Bean Museum, Brigham Young University, Provo, UT, 84602, USA
[5]Department of Biology and School of Global Environmental Sustainability, Colorado State University, Fort Collins, CO, 80523, USA
[6]Canadian High Arctic Research Station, Polar Knowledge Canada, Cambridge Bay, NU, X0B0C0, Canada
[7]School of Science, University of Waikato, Hamilton, 3216, New Zealand
[8]Department of Ecology and Evolutionary Biology and Cooperative Institute for Research in Environmental Science, University of Colorado Boulder, Boulder, CO, 80309, USA

Correspondence to: Melisa A. Diaz (diaz.237@osu.edu)

Abstract. Modeling studies and field mapping show that increases in ice thickness during glacial periods were not uniform across Antarctica. Rather, outlet glaciers that flow through the Transantarctic Mountains (TAM) experienced the greatest changes in ice thickness. As a result, ice-free areas that are currently exposed may have been covered by ice at various points during the Cenozoic, thereby providing a record of past ice sheet behavior. We collected soil surface samples and depth profiles every 5 cm to refusal (up to 30 cm) from eleven ice-free areas along the Shackleton Glacier, a major outlet glacier of the East Antarctic Ice Sheet (EAIS) and measured meteoric ^{10}Be and NO_3^- concentrations to calculate and estimate surface exposure ages. Using ^{10}Be inventories from three locations, calculated maximum exposure ages range from 4.1 Myr at Roberts Massif near the Polar Plateau to 0.11 Myr at Bennett Platform further north. When corrected for inheritance of ^{10}Be from prior exposure, the ages (representing a minimum) range from 0.14 Myr at Roberts Massif to 0.04 Myr at Thanksgiving Valley. We correlate NO_3^- concentrations with meteoric ^{10}Be to estimate exposure ages for all locations with NO_3^- depth profiles but only surface ^{10}Be data. These results indicate that NO_3^- concentrations can be used in conjunction with meteoric ^{10}Be to help interpret EAIS dynamics over time. We show that the Shackleton Glacier has the greatest fluctuations near the Ross Ice Shelf while tributary glaciers are more stable, reflecting the sensitivity of the EAIS to climate shifts at TAM margins.

https://doi.org/10.5194/esurf-2020-50
Preprint. Discussion started: 8 July 2020

1. Introduction

Exposed terrestrial surfaces in Antarctica have previously been used to elucidate glacial history and assess ice sheet stability during warm periods (Balco, 2011; Denton et al., 1993; Mackintosh et al., 2014). While Antarctica is thought to have had a permanent ice sheet since the Eocene, both the East and West Antarctic Ice Sheets (EAIS and WAIS, respectively) have fluctuated in extent and thickness throughout the Cenozoic (Barrett, 2013; DeConto and Pollard, 2016; Huybrechts, 1993). The WAIS has been drastically reduced in size during interglacial periods and there is evidence from ANDRILL marine sediment cores suggesting there have been numerous times over the last 11 Ma with open water in the Ross Embayment (Barrett, 2013; McKay et al., 2009; Shakun et al., 2018). The most recent partial collapse of the WAIS was during the Pleistocene, and the most recent total collapse was during the Pliocene (Naish et al., 2009; Scherer et al., 1998).

The collapse of the WAIS during the Pliocene contributed ~5 m to sea level, but Pliocene sea levels were at least 25 m higher than today, indicating additional water sources, likely from the EAIS and Greenland Ice Sheet (GIS) (Dwyer and Chandler, 2009; Pollard and DeConto, 2009). There is substantial evidence indicating that the WAIS is susceptible to collapse due to warming (Pollard and DeConto, 2009); however, the overall stability of the EAIS has also been questioned (Huybrechts, 1993; Scherer et al., 2016; Sugden, 1996; Wilson, 1995).

Here, we evaluated fluctuations of the EAIS during glacial and potentially interglacial periods. Outlet glaciers are among the most sensitive areas to glaciological change in Antarctica, and changes in their extents over time are recorded in nearby sedimentary deposits (Golledge et al., 2013; Jones et al., 2015; Scherer et al., 2016; Spector et al., 2017). We focus on the Shackleton Glacier, a major outlet glacier of the EAIS. The Shackleton Glacier has several exposed peaks of the Transantarctic Mountains (TAM) along the length of glacier, including at both low and high elevations. We report concentrations of meteoric ^{10}Be and nitrate (NO_3^-) in soils from eleven ice-free areas and use these data to calculate and estimate exposure ages. Our findings contribute to a growing body of work suggesting that some portions of the EAIS are susceptible to rapid advance and retreat.

https://doi.org/10.5194/esurf-2020-50
Preprint. Discussion started: 8 July 2020

2. Background

2.1. Stability of the EAIS

There are two competing hypotheses regarding the stability of the EAIS, though more information from various regions in Antarctica is necessary to fully refute or support either hypothesis. "Stabilists" argue that the EAIS is stable and has not fluctuated in size significantly over the last ~14 Ma (e.g., Denton et al., 1993), while "dynamicists" suggest that the EAIS is dynamic and waxes and wanes (e.g., Webb and Harwood, 1991). Previous studies used a variety of geomorphological and exposure age dating techniques at high elevations (>1000 m) in the McMurdo Dry Valleys (MDV) to assert that the Antarctic interior maintained its aridity and cold-based glaciers since the mid-Miocene (Lewis et al., 2008; Sugden, 1996; Sugden et al., 1993, 1995). These studies suggest major thickening of outlet glaciers but no major ice sheet retreat during the Pliocene (Golledge et al., 2013; Golledge and Levy, 2011; Marchant et al., 1996).

Evidence for a dynamic EAIS is derived primarily from the diamictite rocks (tills) of the Sirius Group, which are found throughout the Transantarctic Mountains and include well-documented outcrops at the Shackleton Glacier. The Sirius Group deposits are characteristic of warm and polythermal based glaciers (Hambrey et al., 2003), but their age is not known. Some of the deposits contain pieces of shrubby vegetation, suggesting that the Sirius Group formed under conditions warmer than present with trees occupying inland portions of Antarctica (Webb et al., 1984, 1996; Webb and Harwood, 1991). Sparse marine diatoms found in the sediments were initially interpreted as evidence for formation of the Sirius Group via glacial over riding of the Transantarctic Mountains during the warmer Pliocene (Barrett et al., 1992), though it is now argued that the marine diatoms were wind-derived contamination, indicating that the Sirius Group is older (Scherer et al., 2016; Stroeven et al., 1996). Following several reviews of the stable versus dynamic EAIS debate, Barrett (2013) concluded that the EAIS maintained polar desert conditions with minimal retreat throughout the Pliocene. More recent models have suggested that portions of the EAIS, particularly outlet glaciers, were and still are susceptible to rapid retreat (DeConto and Pollard, 2016; Scherer et al., 2016). However, the degree of EAIS sensitivity to warming is model-dependent and exposure ages/proxy data are needed to constrain model results (Dolan et al., 2018).

2.2. Cosmogenic nuclide exposure age dating and meteoric ^{10}Be systematics

^{10}Be is a cosmogenic radionuclide with a half-life of 1.39 Ma (Nishiizumi et al., 2007) that is produced both in the atmosphere (meteoric) and *in-situ* in mineral grains. In the atmosphere, N and O gases are bombarded by high energy cosmic radiation to produce meteoric ^{10}Be. Particle reactive ^{10}BeO or $^{10}Be(OH)_2$ is produced and removed from the atmosphere by wet and dry deposition (McHargue and Damon, 1991). At Earth's surface, meteoric ^{10}Be sorbs onto clay particles and is insoluble in most natural waters of pH greater than 4 (Brown et al., 1992; You et al., 1989). Meteoric ^{10}Be accumulation in soils is controlled by surface exposure duration, erosion, clay particle translocation, solubility, and sedimentation. Thus, meteoric ^{10}Be can be used as a tool to understand exposure age, erosion rates, and soil residence times (see Willenbring and Von Blanckenburg, 2009 and references within).

The measurement and use of meteoric ^{10}Be has enabled researchers to date surfaces and features which otherwise lack sufficient coarse-grained quartz for *in-situ* ^{10}Be analysis. Previous studies have measured meteoric ^{10}Be in MDV and Victoria Land soils and sediments to calculate exposure ages and determine the onset of the current polar desert regime (Dickinson et al., 2012; Graham et al., 2002; Schiller et al., 2009; Valletta et al., 2015). These previous studies generally show that high elevation, northern fringe regions along the Ross Embayment have been hyper-arid since at least the Pliocene. Meteoric ^{10}Be data have yet to be published from the central Transantarctic Mountains (CTAM), which represent ice sheet dynamics closer to the Polar Plateau.

Here, we used meteoric ^{10}Be to estimate CTAM relative exposure ages, acknowledging the widespread use of *in-situ* exposure age dating which we later use for cross-validation. *In-situ* cosmogenic nuclides, such as ^{10}Be, ^{26}Al, ^{21}Ne, and ^{3}He, have been used to determine surface exposure ages at several locations across Antarctica, particularly in the MDV and other exposed surfaces in Victoria Land (e.g. (Balco et al., 2019; Brook et al., 1993, 1995; Bruno et al., 1997; Ivy-Ochs et al., 1995; Strasky et al., 2009). There are considerably fewer studies from the CTAM (e.g., Ackert and Kurz, 2004; Balter et al., 2020; Bromley et al., 2010; Kaplan et al., 2017; Spector et al., 2017). Exposure ages of CTAM tills and boulders from those previous studies ranged from <10 ka to >14 Ma, and their results suggest that the EAIS may have maintained persistent arid conditions since as early as the Miocene. . However, many of these age-date estimates were inferred from samples

https://doi.org/10.5194/esurf-2020-50
Preprint. Discussion started: 8 July 2020

collected at the glacier heads and may not encompass fluctuations near the glacier terminus. Additionally, *in-situ* dating relies on the occurrence of coarse-grained minerals (usually quartz) in rocks and boulders, and thus is spatially limited.

3. Study sites

Shackleton Glacier (~84.5 to 86.4°S; ~130 km long and ~10 km wide) is a major outlet glacier of the EAIS which drains north into the Ross Embayment with other CTAM outlet glaciers to form the Ross Ice Shelf (RIS) (Fig. 1). The ice flows between exposed surfaces of the Queen Maud Mountains, which range from elevations of ~150 m near the RIS to >3,500 m further inland. The basement geology of the Shackleton Glacier region is comprised of igneous and metamorphic rocks formed from intruded and metamorphosed sedimentary and volcanic strata during the Ross Orogeny (450-520 Ma) (Elliot and Fanning, 2008). The southern portion of the region consists of the Devonian-Triassic Beacon Supergroup and Jurassic Ferrar Group, while the northern portions consists of Pre-Devonian granitoids and the Early to Mid-Cambrian Taylor Group (Elliot and Fanning, 2008; Paulsen et al., 2004). These rocks serve as primary weathering products for soil formation (Claridge and Campbell, 1968). Deposits of the Sirius Group, the center of the stable vs. dynamic EAIS debate, have been previously identified in the southern portion of the Shackleton Glacier region, particularly at Roberts Massif (Fig. 2) and Bennett Platform, with a small exposure at Schroeder Hill (Hambrey et al., 2003).

The valleys and other ice-free areas within the region have been modified by the advance and retreat of the Shackleton Glacier, smaller tributary glaciers, and alpine glaciers. Similar to the Beardmore Glacier region, the Shackleton Glacier region is a polar desert, which results in high rates of salt accumulation in soils. The surface is comprised primarily of till, weathered primary bedrock, and scree, which range in size from small boulders and cobbles to sand and silt. Clays have been previously identified in all samples from Roberts Massif and are likely ubiquitous throughout the region (Claridge and Campbell, 1968). However, the clays are a mixture of those derived from sedimentary rocks and contemporaneous weathering (Claridge and Campbell, 1968). Thin, boulder belt moraines, characteristic of cold-based glaciers, were deposited over bedrock and tills at Roberts Massif, while large moraines were deposited at Bennett Platform, characteristic of warm or polythermal glacial dynamics (Fig. 2, Balter et al., 2020; Claridge and Campbell, 1968).

https://doi.org/10.5194/esurf-2020-50
Preprint. Discussion started: 8 July 2020

4. Methods

4.1. Sample collection

During the 2017-2018 austral summer, we visited eleven ice-free areas along the Shackleton Glacier: Roberts Massif, Schroeder Hill, Bennett Platform, Mt. Augustana, Mt. Heekin, Thanksgiving Valley, Taylor Nunatak, Mt. Franke, Mt. Wasko, Nilsen Peak, and Mt. Speed (Fig. 1). Two samples (Table 1) were collected at each location (except for Nilsen Peak and Mt. Wasko, represented by only one sample) with a plastic scoop and stored in Whirl-Pak™ bags. One sample was collected furthest from the Shackleton Glacier or other tributary glaciers (within ~2,000 m) in a transect to represent soils that were likely exposed during the Last Glacial Maximum (LGM) and previous recent glacial periods. A second sample was collected closer to the glacier (between ~1,500 and 200 m from the first sample) to represent soils likely to have been exposed by more recent ice margin retreat.

Soil pits were dug by hand at the sampling locations furthest from the glacier for Roberts Massif, Schroeder Hill, Mt. Augustana, Bennet Platform, Mt. Heekin, Thanksgiving Valley, and Mt. Franke. Continuous samples were collected every 5 cm until refusal (up to 30 cm) and stored frozen in Whirl-Pak™ bags. All surface (21) and depth profile (25) samples were shipped frozen to The Ohio State University and kept frozen until analyzed.

4.2. Analytical methods

4.2.1. Meteoric ^{10}Be analysis

A total of 30 sub-samples of surface soils from all locations and depth profiles from Roberts Massif, Bennett Platform, and Thanksgiving Valley were sieved to determine the grain size at each location. The percentages of gravel (>2 mm), sand (63-425µm), and silt (<63µm) are reported in Table S1. Since there is a strong grain size dependence of meteoric ^{10}Be where very little ^{10}Be is carried on coarse (>2 mm) grains (Pavich et al., 1986), the gravel portion of the sample was not included in the meteoric ^{10}Be analysis. The remaining soil (<2 mm) was ground to fine powder using a shatterbox.

Meteoric ^{10}Be (Table 2) was extracted and purified at the NSF/UVM Community Cosmogenic Facility following procedures originally adapted and modified from Stone (1998). First, 0.5 g of powdered soil was weighed into platinum crucibles and 0.4 g of SPEX ^{9}Be carrier (with a concentration of 1,000 µg mL^{-1}) was added to each sample. The samples were fluxed with a mixture of potassium hydrogen fluoride and sodium sulfate. Perchloric acid was then added to remove potassium by precipitation and later evaporated. Samples were dissolved in nitric acid and precipitated as beryllium hydroxide ($Be(OH)_2$) gel, then packed into stainless steel cathodes for accelerator mass spectroscopy isotopic analysis at the Purdue Rare Isotope Measurement Laboratory (PRIME Lab). Isotopic ratios were normalized to primary standard 07KNSTD with an assumed ratio of 2.85 x 10^{-12} (Nishiizumi et al., 2007). We corrected sample ratios with a $^{10}Be/^{9}Be$ blank ratio of 8.2 ± 1.9 x 10^{-15}, which is the average and standard deviation of two blanks processed alongside the samples. We subtracted the blank ratio from the sample ratios and propagated uncertainties in quadrature.

4.2.2. Nitrate analysis

Separate, un-sieved sub-samples of soil from all locations and depth profiles were leached at a 1:5 soil to water ratio for 24 hours, then filtered through a 0.4 µm Nucleopore membrane filter. The leachate was analyzed on a Skalar San++ Automated Wet Chemistry Analyzer with a SA 1050 Random Access Auto-sampler (Lyons et al., 2016; Welch et al., 2010). Concentrations are reported as NO_3^- (Table S2) with accuracy, as determined using USGS 2015 standard, and precision better than 5% (Lyons et al., 2016).

4.3. Exposure age model

We developed a mass balance using the fluxes of meteoric ^{10}Be in and out of Shackleton Glacier region soils to calculate the amount of time which has passed since the soil was exposed (Pavich et al., 1984, 1986). The model assumes that soils that were overlain by glacial ice in the past, and are now exposed, accumulated a lower surface concentration and inventory of ^{10}Be than soils that were exposed throughout the glacial period (Fig. 3). The concentration of meteoric ^{10}Be at the surface (N, atoms g^{-1}) per unit of time (dt) is expressed as a function (Eq. 1), where the addition of ^{10}Be is represented as the atmospheric flux to the surface (Q, atoms cm^{-2} yr^{-1}) and the removal is due to radioactive decay, represented by a disintegration constant (λ, yr^{-1}) and erosion (E, cm yr^{-1}) with respect to soil density (ρ, g cm^{-3}).

$$\frac{dN}{dt} = Q - \lambda N - \frac{E\rho N}{dz} \quad (1)$$

However, this function is highly dependent on dz, which represents an unknown value of depth into the soil column which is influenced by meteoric ^{10}Be deposition and removal. We can account for this uncertainty and other uncertainties

https://doi.org/10.5194/esurf-2020-50
Preprint. Discussion started: 8 July 2020

regarding ^{10}Be migration in the soil column by calculating the inventory (I, atoms cm^{-2}) of the soil (Eq. 2), assuming that Q has not changed systematically over the accumulation interval (Graly et al., 2010; Pavich et al., 1986).

$$I = \sum N \cdot \rho \cdot dz \quad (2)$$

If we know the inventory of meteoric ^{10}Be in the soil profile, the concentration at the surface, and soil density, and use published values for erosion and ^{10}Be flux to the surface, we can combine Eq. (1) and Eq. (2), and solve for time (t, years) (Eq. 3).

$$t = -\frac{1}{\lambda} \cdot \ln\left[1 - \frac{I\lambda}{Q - E\rho N}\right] \quad (3)$$

Equation (3) provides a maximum exposure age assuming that soil profile did not have meteoric ^{10}Be before it was exposed to the surface ($N_0 = 0$). Since our exposure age dating technique relies on the number of atoms within the sediment column (I), any pre-existing ^{10}Be atoms in the soil ($N_0 \neq 0$) cause the calculated age to be an overestimate (Fig. 3c-d) (Graly et al., 2010). Meteoric ^{10}Be concentrations typically decrease with depth until they reach a "background" level (Graly et al., 2010). We can use that background value to calculate an initial inventory, also referred to as inheritance (I_i, atoms cm^{-2}) using Eq. (4), where N_z is the ^{10}Be concentration (atoms g^{-1}) at the bottom of the profile (z, cm), and correct the observed inventory (Eq. 5). However, an accurate I_i can only be determined for soil profiles which have a decrease in ^{10}Be concentrations to background levels due to the downward transport of ^{10}Be from the surface. This may not be the case in areas of permafrost where ^{10}Be is restricted to the active layer (Bierman et al., 2014).

$$I_i = N_z \cdot \rho \cdot z \quad (4)$$

$$t = -\frac{1}{\lambda} \cdot \ln\left[1 - \frac{(I - I_i)\lambda}{Q - E\rho N}\right] \quad (5)$$

4.3.1. Model variable selection

The exposure age calculations are dependent on the selected values for the variables in Eq. (1-5). We chose a flux value (Q) of 1.3 x 10^5 atoms cm^{-2} yr^{-1} from Taylor Dome (Steig et al., 1995) due to a similar climate to that of the CTAM and an absence of local meteoric ^{10}Be flux data. While we did not calculate erosion rates, previous studies have estimated

https://doi.org/10.5194/esurf-2020-50
Preprint. Discussion started: 8 July 2020

rates from rocks of 1 to 65 cm Myr^{-1} in Victoria Land (Ivy-Ochs et al., 1995; Margerison et al., 2005; Morgan et al., 2010; Strasky et al., 2009; Summerfield et al., 1999) and 5 to 35 cm Myr^{-1} further south in the Transantarctic Mountains (Ackert and Kurz, 2004; Balter et al., 2020; Morgan et al., 2010). Balter et al. (2020) determined that erosion rates for boulders at Roberts Massif which were less than 2 cm Myr^{-1}. However, we chose a conservative value of 5 cm Myr^{-1} for the Shackleton Glacier region. Soil density (ρ) across the Shackleton Glacier region was approximately 2 g cm^{-3}.

5. Results

5.1. Surface concentrations of meteoric ^{10}Be and grain size

Surface concentrations of meteoric ^{10}Be span more than an order of magnitude and range from 2.9 x 10^8 atoms g^{-1} at Mount Speed to 73 x 10^8 atoms g^{-1} at Roberts Massif (Fig. 4). At individual sites where samples were collected at two locations, concentrations are typically highest for the samples furthest from the glacier, with notable exceptions at Roberts Massif and Thanksgiving Valley. In general, concentrations of meteoric ^{10}Be increase with both distance from the coast and elevation (Fig. 5). There is a stronger relationship with distance from the coast (R^2 = 0.48), compared to elevation (R^2 = 0.39). An exception to this trend is Bennett Platform as both surface samples from Bennett Platform have lower concentrations than expected from the linear regression. If the samples from Bennett Platform are excluded from the linear regression, the R^2 values increase to 0.67 and 0.51 for distance from the coast and elevation, respectively, with p-values < 0.001 for both regressions.

Sediment grain size is similar among the three soil profiles from Roberts Massif, Bennett Platform, and Thanksgiving Valley; the soils are primarily comprised of sand-sized particles, with less silt-sized and smaller material (Fig. 6). The proportions of silt and gravel are similar at Roberts Massif, although the majority of the profile is sand-sized. Thanksgiving Valley has the least fine material, while Bennett Platform has a more even grain size distribution.

5.2. Calculated maximum and inheritance-corrected exposure ages

Calculated maximum meteoric ^{10}Be exposure ages for Roberts Massif, Bennett Platform, and Thanksgiving Valley range from 0.11 Myr at Bennett Platform to 4.1 Myr at Roberts Massif, assuming no inheritance (Table 3). Bennett Platform is the only location that has exponentially decreasing ^{10}Be concentrations with depth and appears to approach background levels towards the bottom of the 15 cm deep profile. We used the 10-15 cm ^{10}Be concentration value to calculate the inheritance for this location. While ^{10}Be concentrations at Roberts Massif and Thanksgiving Valley did not exponentially decrease in a similar manner, we used the lowest concentration from each of the profiles to calculate the inheritance, which is likely an overestimate. Using Eq. (5), the inheritance-corrected exposure ages are younger and range from 0.04 Myr at Thanksgiving Valley to 0.14 Myr at Roberts Massif (Table 3). These corrected ages are minimum ages.

5.3. Estimated exposure ages for sites without meteoric ^{10}Be depth profiles

5.3.1 Maximum and inheritance-corrected estimated ages using NO_3^- concentrations

Meteoric ^{10}Be and NO_3^- concentrations are correlated in the depth profiles from Roberts Massif, Bennett Platform, and Thanksgiving Valley, with a strong power relationship between the two measurements (R^2 = 0.66 to 0.99) (Fig. 7c). In addition, similar to the meteoric ^{10}Be profiles, the NO_3^- concentrations are highest for the samples which were collected furthest from the coast and at the highest elevations (Table S2).

We used the relationship between NO_3^- and ^{10}Be to estimate ^{10}Be concentrations for all seven soil profiles (Table 3, Fig. 8). The calculated and NO_3^- estimated maximum exposure ages only differ by ~6-20% for Roberts Massif, Bennett Platform, and Thanksgiving Valley, which have full data sets for both parameters. The inheritance-corrected exposure ages have a difference of ~10-35% between the calculated and estimated ages. Since we could not calculate ^{10}Be exposure ages for the profiles from Schroeder Hill, Mt. Augustana, Mt. Heekin, and Mt. Franke, we were not able to make similar comparisons. However, we were able to compare the estimated surface ^{10}Be concentrations using NO_3^- to the measured ^{10}Be concentrations. The percent differences at Schroeder Hill and Mt. Heekin are 4% and 7%, respectively, while Mt. Augustana and Mt. Franke have higher differences of 36% and 40%, respectively (Tables 3 and 4).

5.3.2 Maximum estimated ages inferred using maximum meteoric ^{10}Be concentrations

Similar to our exposure age estimates using NO_3^- concentrations, we used the relationship between the maximum meteoric ^{10}Be concentration in the soil profile and the meteoric ^{10}Be inventory (Graly et al., 2010) to infer ^{10}Be inventories and estimate maximum exposure ages (without a correction for inheritance) for all eleven locations (Table 4, Fig. 8). As is the case for Roberts Massif and Thanksgiving Valley, the highest concentrations may not always be at the surface for all locations; however, the relationship is sufficiently strong to provide an estimate of the ^{10}Be inventory and thus an age estimate (Fig. S1). Compared to the measured inventories from Roberts Massif, Bennett Platform, and Thanksgiving Valley, the inferred inventories differ by ~3-18%. The estimated inferred maximum exposure ages range from 0.13 Myr at Mt. Speed to >14 Myr at Roberts Massif. With the exception of Roberts Massif and Thanksgiving Valley, the oldest surfaces are those which we sampled furthest from the glacier. The sample from Roberts Massif collected closest to the glacier has an estimated exposure age that is outside the model limits (>14 Myr). The calculated maximum ages and estimated maximum ages from the inferred inventory differ by ~40% for Roberts Massif and Thanksgiving Valley, and the estimated age is half the calculated age for Bennett Platform (Table 4).

6. Discussion

6.1. Calculated and estimated exposure age validation

The Shackleton Glacier region soil profiles have the highest meteoric ^{10}Be concentrations (~10^9 atoms g^{-1}) yet measured in Earth's polar regions (Fig. 7a). Though our profiles are shallower than profiles from the MDV and Victoria Land in Antarctica (Dickinson et al., 2012; Schiller et al., 2009; Valletta et al., 2015) and Sweden and Alaska in the Arctic (Bierman et al., 2014; Ebert et al., 2012), the soils from these previous studies reached background concentrations of ^{10}Be within the top 40 cm, which is close to our maximum depth of 30 cm at Thanksgiving Valley. Bennett Platform is most similar to the soil profiles from other regions in Antarctica, as they have decreasing ^{10}Be concentrations with depth, while Thanksgiving Valley and Roberts Massif are relatively homogenous and more similar to profiles from the Arctic. As a result, our profiles are likely sufficient for inventory and inheritance calculations.

Our calculated and estimated exposure ages are consistent with the limited *in-situ* exposure age data from the Shackleton Glacier region (http://antarctica.ice-d.org; Balco, 2020). From *in-situ* ^{10}Be, ^{26}Al, ^{3}He, and ^{21}Ne data, exposure ages on the northern flank of Roberts Massif range from ~0.33 to 1.58 Myr (Balter et al., 2020; ICE-D), and our inheritance-corrected calculated age was 0.14 Myr, with a maximum (un-corrected) value of 4.09 Myr. The inheritance-corrected NO_3^- estimated age is 0.17 Myr. To the north, the *in-situ* ages from Thanksgiving Valley vary greatly from ~4.3 kyr to 0.45 Myr, though most ages appear to be around 35 kyr (ICE-D), which is close to our inheritance-corrected calculated and NO_3^-

https://doi.org/10.5194/esurf-2020-50
Preprint. Discussion started: 8 July 2020

estimated ages of ~40 kyr and ~30 kyr, respectively. Closer to the Ross Ice Shelf, the *in-situ* ages from Mt. Franke range from ~29 kyr to 0.19 Myr, which is similar to our NO_3^- estimated ages, which range from ~18 kyr for the inheritance-corrected age to a maximum age of 0.23 Myr.

The *in-situ* ages are youngest closer to the glacier at nearly all locations along the Shackleton Glacier (Balter et al., 2020; ICE-D), which is the same trend we observed for the meteoric ^{10}Be ages. In addition, the *in-situ* ages and calculated and estimated ages from the Shackleton Glacier region are typically younger at lower elevations and decrease closer to the Ross Ice Shelf (Fig. 8). Similar patterns have been observed in the Beardmore Glacier region. Exposure ages at the head of the Beardmore Glacier at the Meyer Desert are the oldest (up to 5.0 Myr). However, on the western side near the Beardmore Glacier, the ages are only ~10 kyr (Ackert and Kurz, 2004). To the north, ages from Cloudmaker range from ~9 kyr to 15 kyr near the glacier, and ~ 600 to 3 kyr near the Ross Ice Shelf at Mt. Hope (Spector et al., 2017). We argue that while the maximum calculated and estimated exposure ages can indicate general trends in exposure ages and are useful in establishing an upper age limit, they are likely an overestimate and the inheritance-corrected (minimum) ages are more accurate, as determined by comparison to previous work.

6.2. NO_3^- as an efficient exposure age dating tool

This study is not the first to attempt to use water-soluble NO_3^- to help understand glacial history, but it is the first use NO_3^- concentrations to directly estimate meteoric ^{10}Be concentrations. Previous studies have argued that atmosphere-derived salt concentrations at the surface may correlate with exposure ages and wetting ages in Antarctica (Graham et al., 2002; Graly et al., 2018; Lyons et al., 2016; Schiller et al., 2009). Graly et al. (2018) showed that, in particular, water-soluble NO_3^- and boron exhibited the strongest relationships (R^2 = 0.9 and 0.99, respectively). Lyons et al. (2016) used nitrate concentrations to estimate the amount of time since the soils were last wetted and Graham et al. (2002) attempted to calculate exposure ages using the inventory of nitrate in the soil. Graly et al. (2018) argue that boron is preferable to nitrate due to concerns over nitrate mobility under sub-arid conditions (e.g. Frey et al., 2009; Michalski et al., 2005), and given that uncertainties in local accumulation rates and ion transport can result in inaccurate ages when using NO_3^- alone (Graham et al., 2002; Schiller et al., 2009). Based on the results presented here for hyper-arid CTAM ice-free regions and the concerns

https://doi.org/10.5194/esurf-2020-50
Preprint. Discussion started: 8 July 2020

with boron mobility depending on whether the B species present in the soils is BO_3^{3-} (borate) or H_3BO_3 (boric acid), we conclude that NO_3^- appears suitable for relative age dating and producing age estimates.

Through a coupled approach using both meteoric ^{10}Be and NO_3^- concentrations, we developed a useful model for estimating soil exposure ages. We show that the percent differences between calculated and NO_3^- estimated ages are low (see Section 4.4.) and argue that the relationship between meteoric ^{10}Be and NO_3^- can be used to expand our current exposure age database for the TAM; compared to cosmogenic radionuclide analyses, NO_3^- analyses are rapid and cost effective. However, a model using NO_3^- or salts alone is likely insufficient, unless the anion accumulation rates are known (Graham et al., 2002; Schiller et al., 2009). Though the regressions between NO_3^- and ^{10}Be are strong (Fig. 7c), each of the three profiles from Roberts Massif, Bennett Platform, and Thanksgiving Valley have different regression coefficients and slopes. In other words, the relationship between meteoric ^{10}Be and NO_3^- is not uniform across the Shackleton Glacier region and varies depending on the location, likely due to local glacial history and climate, soil development, and geography. To address these uncertainties, some ^{10}Be data, surface samples for all locations and a few depth profiles in particular, are necessary to choose the proper regression to minimize the associated error.

We tested our meteoric ^{10}Be – NO_3^- model with data from Arena Valley (Graham et al., 2002) and found that our model is roughly applicable to other TAM ice-free areas. The power relationship between ^{10}Be and NO_3^- throughout the profile is not as strong for the Arena Valley samples compared to Shackleton Glacier samples; there is stronger correlation in the top 20 cm ($R^2 = 0.61$) than the bottom 70 cm ($R^2 < 0.01$). The estimated inventory is 7.22×10^9 atoms cm^{-2}, while the calculated inventory is 1.3×10^{10} atoms cm^{-2}, and the exposure ages (without erosion and inheritance corrections) are 56 kyr and 87 kyr, respectively. Though our inheritance-corrected NO_3^- estimated ages are validated using *in-situ* data from previous studies, until our estimated exposure dating technique can be tested more broadly, we interpret these ages as relative or estimated ages.

6.3. Implications for ice sheet dynamics

Sirius Group deposits were only observed at Roberts Massif (Fig. 2a) and were either deposited or exposed as the Shackleton Glacier retreated in this region. At sample site RM2-8, where soil collected closest to the Shackleton Glacier, we

https://doi.org/10.5194/esurf-2020-50
Preprint. Discussion started: 8 July 2020

documented a large diamictite that is underlain by soils estimated to be a maximum of >14 Myr in age. While this soil age is likely an overestimate given previously published *in-situ* ages (Balter et al., 2020), the Sirius Group was not observed near the relatively younger RM2-1 soils, with an inheritance-corrected age of 0.14 Myr. We interpret these sparse data to suggest that either the tills were transported from further inland during previous glacial retreat, or that the Sirius Group formed over an extended period of time. However, considering we did not observe any diamictite on younger soils, these observations support previous studies (e.g. Barrett, 2013; Sugden et al., 1993, 1995; Sugden, 1996), which argue that, at least for the southern Shackleton Glacier region, the Sirius Group likely formed prior to the Pliocene.

Our data support models and previous studies suggesting that EAIS advance and retreat was not synchronous during the LGM and throughout the late Cenozoic (DeConto and Pollard, 2016; Golledge et al., 2013; Marchant et al., 1994; Scherer et al., 2016). Calculated and estimated exposure ages (including both maximum and inheritance-corrected) are youngest near the coast and greatest at the head of the Shackleton Glacier (Fig. 8). The furthest inland sample at Mt. Franke indicates that deglaciation occurred as recently as ~0.02 Myr in the northern portion of the region, although the samples closest to the glacier are likely younger in age and may indicate that deglaciation continued into the late Pleistocene/ early Holocene (Spector et al., 2017). Deglaciation in the southern portion of the region likely occurred earlier, with the furthest inland samples from Roberts Massif, Schroeder Hill, and Bennett Platform exposed since shortly before or after the onset of the last glacial period (~0.10 Myr) (Blunier and Brook, 2001; Clark et al., 2009; Mackintosh et al., 2014). Previous data from Roberts Massif also suggests that much, if not all of this location was ice-free throughout the last glacial period (Balter et al., 2020). However, our inferred maximum estimated ages also indicate that, similar to the more northern locations, the samples collected closest to the glacier are likely younger and were more recently exposed due to ice retreat (Fig. 8).

Tributary glaciers in the Shackleton Glacier region appear to behave differently than the Shackleton Glacier itself. This is best demonstrated by the Bennett Platform samples, collected near the tributary Gallup Glacier. Bennett Platform is unique in being the only location we sampled with large lateral moraines and several nearby medial moraines (Fig. 2c). The surface concentration of meteoric ^{10}Be is lower at Bennett Platform than what would be expected from regression models relating concentration with elevation and distance from the coast (Fig. 5). The lower concentrations of ^{10}Be, in turn, result in

https://doi.org/10.5194/esurf-2020-50
Preprint. Discussion started: 8 July 2020

relatively lower calculated and estimated exposure ages (Fig. 8; Table 3). Specifically, the exposure ages suggest that glacier retreat following termination of the last glacial period was delayed at Bennett Platform.

We argue that the younger than anticipated exposure age is due to differing glacial dynamics between tributary and major outlet glaciers. Meteoric ^{10}Be concentrations and exposure ages at Mt. Augustana are also lower than anticipated given its distance from the coast and elevation. Similar to Bennett Platform, Mt. Augustana is along a tributary glacier, McGregor Glacier. We did not observe the same large moraines from Bennett Platform, but it is possible that McGregor Glacier and Gallup Glacier behave similarly and have a comparatively delayed response to the transition from glacial to interglacial periods. Previous work in the Royal Society Mountains found that marine and land-terminating glaciers behave asynchronously; although sea-level rise likely induced grounding line retreat in the Ross Sea following the LGM, alpine glaciers have since advanced (Higgins et al., 2000; Jackson et al., 2018). The Shackleton Glacier is marine terminating and likely susceptible to ice shelf stability and sea level rise, while the regional tributary glaciers are likely grounded on bedrock troughs and are resulting more stable with respect to changes in climate. Though the physical properties of Gallup and McGregor Glaciers are unknown during the LGM and previous glacial periods (i.e. cold vs. polythermal, shallow vs. deep grounding), these glaciers possibly represent the dynamics of other tributary glaciers in the CTAM, which may similarly have a delayed response to climate shifts.

7. Conclusions

We measured concentrations of meteoric ^{10}Be and NO_3^- in soils from eleven ice-free areas along the Shackleton Glacier, Antarctica, which include the highest measured meteoric ^{10}Be concentrations from the polar regions. Calculated maximum and inheritance-corrected (minimum) exposure ages are well-correlated with estimated ages, determined using NO_3^- concentrations and inferred ^{10}Be inventories. In particular, coupling NO_3^- concentrations with ^{10}Be measurements represents an efficient method to attain a greater number of exposure ages in the CTAM, a region with currently sparse data. However, while the relationship between NO_3^- and ^{10}Be is strong in the Shackleton Glacier region, its widespread applicability has yet to be addressed.

Soil exposure ages are generally youngest at lower elevations and closer to the Ross Ice Shelf, but are also younger closer to the Shackleton Glacier or other tributary glaciers. Though we could only estimate maximum inferred ages, our soil transects likely encompass the LGM transition. Inheritance-corrected calculated and estimated ages at Roberts Massif (~1 km from the glacier) indicate that the Shackleton Glacier was likely present in its current form since at least the Pleistocene in southern portions of the region. More northern samples indicate that towards the glacier terminus, the Shackleton Glacier is more susceptible to changes in climate and has likely retreated in the past. However, tributary glaciers likely had a delayed retreat following the LGM. These data represent a comprehensive analysis of meteoric ^{10}Be to demonstrate the dynamic behavior of CTAM outlet glaciers at glacier termini and stability at glacier heads.

https://doi.org/10.5194/esurf-2020-50
Preprint. Discussion started: 8 July 2020

Author Contributions

The project was designed and funded by BJA, DHW, IDH, NF, and WBL. Fieldwork was conducted by BJA, DHW, IDH, NF, and MAD. LBC, PRB, and MAD prepared the samples for meteoric ^{10}Be analysis and MAD analyzed the samples for NO_3^-. MAD wrote the article with contributions and edits from all authors.

Data Availability Statement

The datasets generated for this study are included in the article or supplementary materials.

Competing Interests

The authors declare that they have no conflict of interest.

Acknowledgments

We thank the United States Antarctic Program (USAP), Antarctic Science Contractors (ASC), Petroleum Helicopters Inc. (PHI), and Marci Shaver-Adams for logistical and field support. We especially thank Dr. Marc Caffe and the Purdue University PRIME Lab for their assistance with AMS measurements. Additionally, we thank Dr. Andrew Christ at University of Vermont for thoughtful discussions and Dr. Sue Welch and Daniel Gilbert at The Ohio State University for help with initial laboratory analyses. This work was supported by NSF OPP grants 1341631 (WBL), 1341618 (DHW), 1341629 (NF), 1341736 (BJA), NSF GRFP fellowship 60041697 (MAD), and a PRIME Lab seed proposal (MAD). Sample preparation and LBC's time supported by NSF EAR 1735676. Geospatial support for this work provided by the Polar Geospatial Center under NSF OPP grants 1043681 and 1559691.

https://doi.org/10.5194/esurf-2020-50
Preprint. Discussion started: 8 July 2020

Figures:

Figure 1: Overview map of the Shackleton Glacier region, located in the Queen Maud Mountains of the Central Transantarctic Mountains. The red circles represent our eleven sampling locations, with an emphasis on Roberts Massif (orange), Bennett Platform (green), and Thanksgiving Valley (blue), which have the most comprehensive dataset in this study. The bedrock serves as primary weathering product for soil formation (Elliot and Fanning, 2008; Paulsen et al., 2004). Base maps provided by the Polar Geospatial Center.

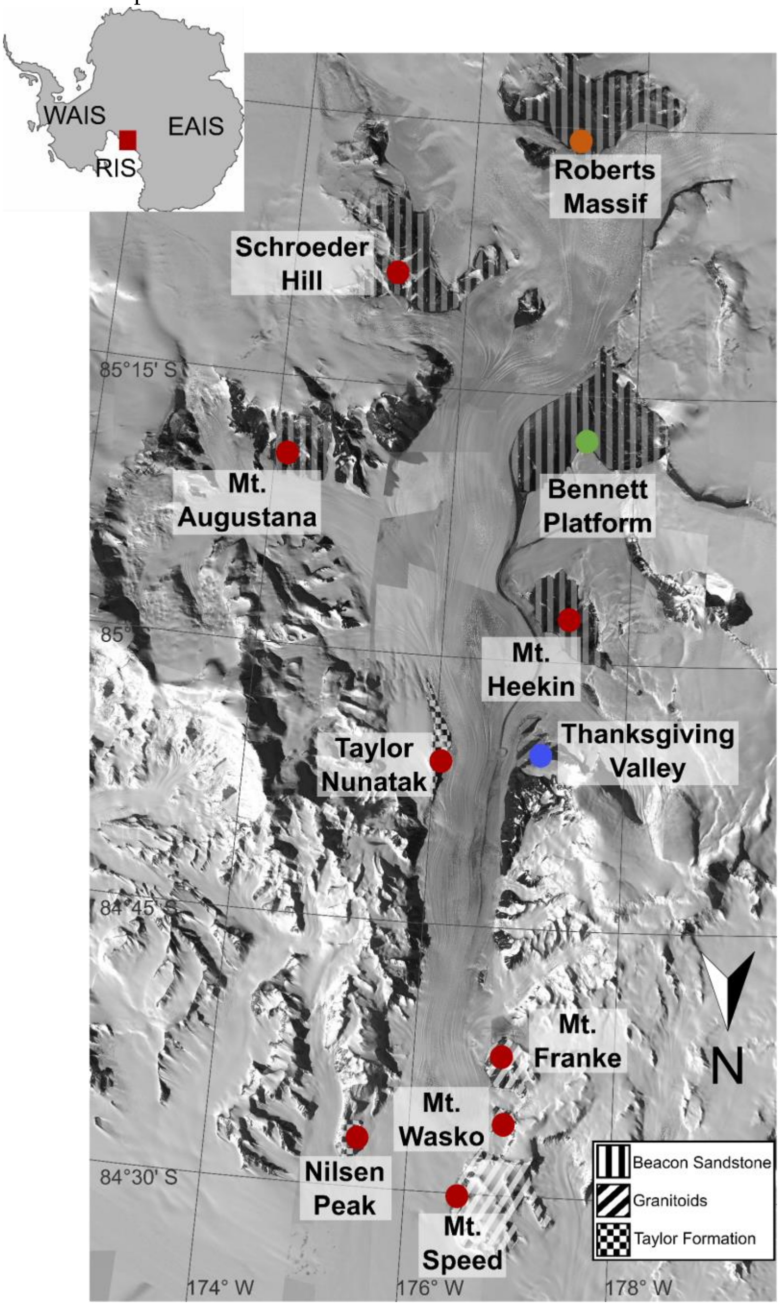

https://doi.org/10.5194/esurf-2020-50
Preprint. Discussion started: 8 July 2020

Earth Surface Dynamics Discussions
Open Access
EGU

Figure 2: The Sirius Group was documented at Roberts Massif near the RM2-8 sampling location (a). Cold-based glacier moraines were observed at Roberts Massif (b) and large polythermal moraines were observed at Bennett Platform (c).

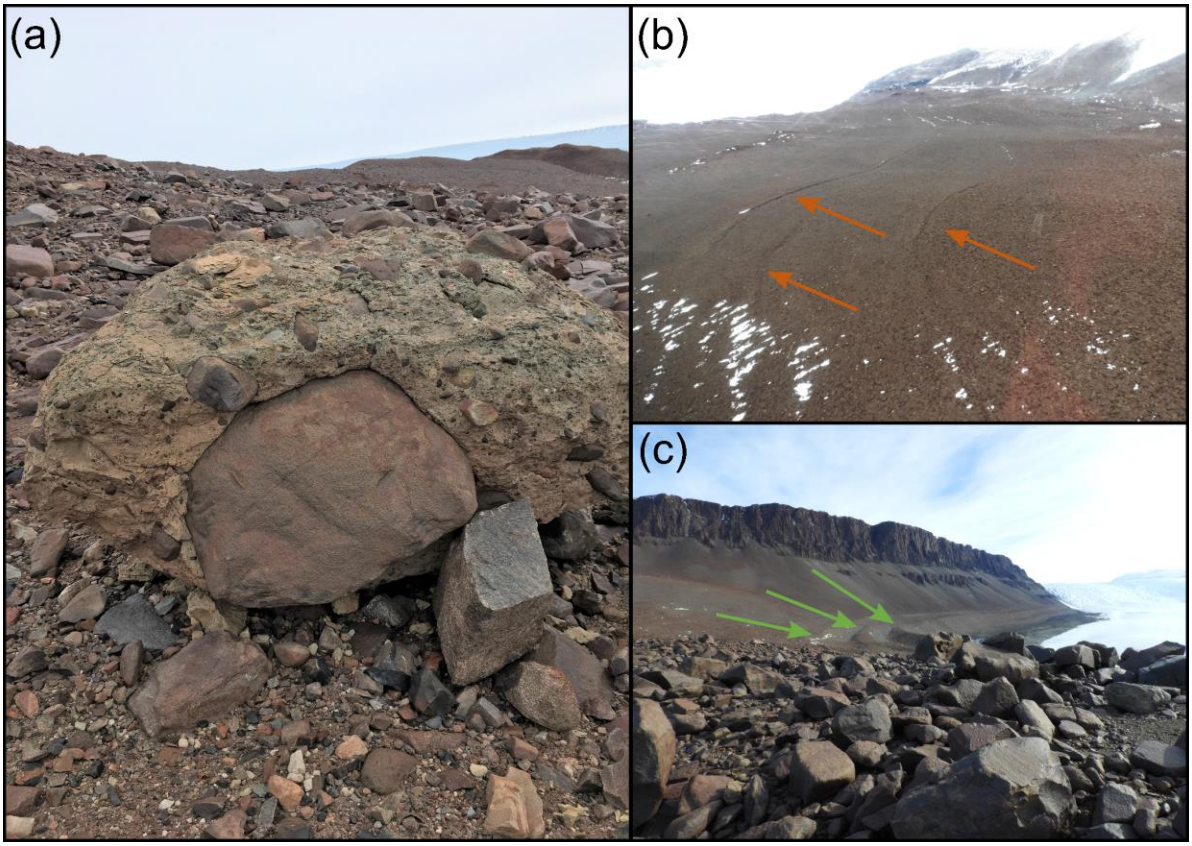

https://doi.org/10.5194/esurf-2020-50
Preprint. Discussion started: 8 July 2020

Figure 3: Conceptual diagram of meteoric ^{10}Be accumulation in soils during glacial advance and retreat. In "ideal" conditions, ^{10}Be accumulates in exposed soils and ^{10}Be concentrations beneath the glacier are negligible (a). As the glacier retreats, ^{10}Be can begin accumulating in the recently exposed soil and an inventory can be measured to calculate exposure ages. In the case where the glacier has waxed and waned numerous times and the soils already contain a non-negligible background concentration of ^{10}Be, inventories need to be corrected for ^{10}Be inheritance (c-d).

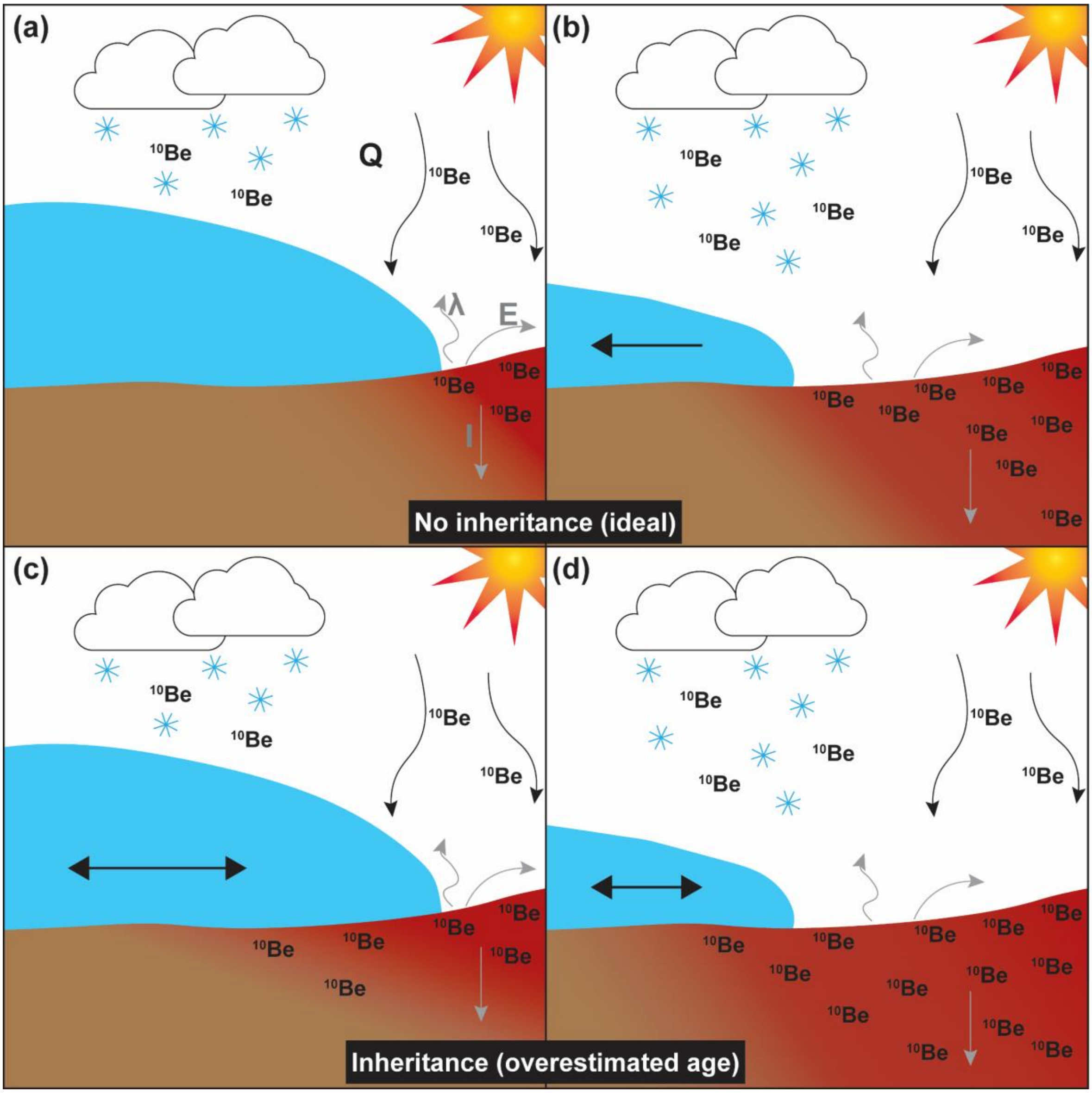

https://doi.org/10.5194/esurf-2020-50
Preprint. Discussion started: 8 July 2020

Figure 4: Spatial distribution of surface meteoric ^{10}Be concentrations in the Shackleton Glacier region. Where possible, two samples were collected at each location to represent surfaces closest to the glacier, which might have been glaciated during recent glacial periods, and samples furthest from the glacier that are likely to have been exposed during recent glacial periods. Insets of Roberts Massif (orange), Bennett Platform (green), and Thanksgiving Valley (blue) are included (color scheme consistent throughout), as these locations serve as the basis for our relative exposure age models. Base maps provided by the Polar Geospatial Center.

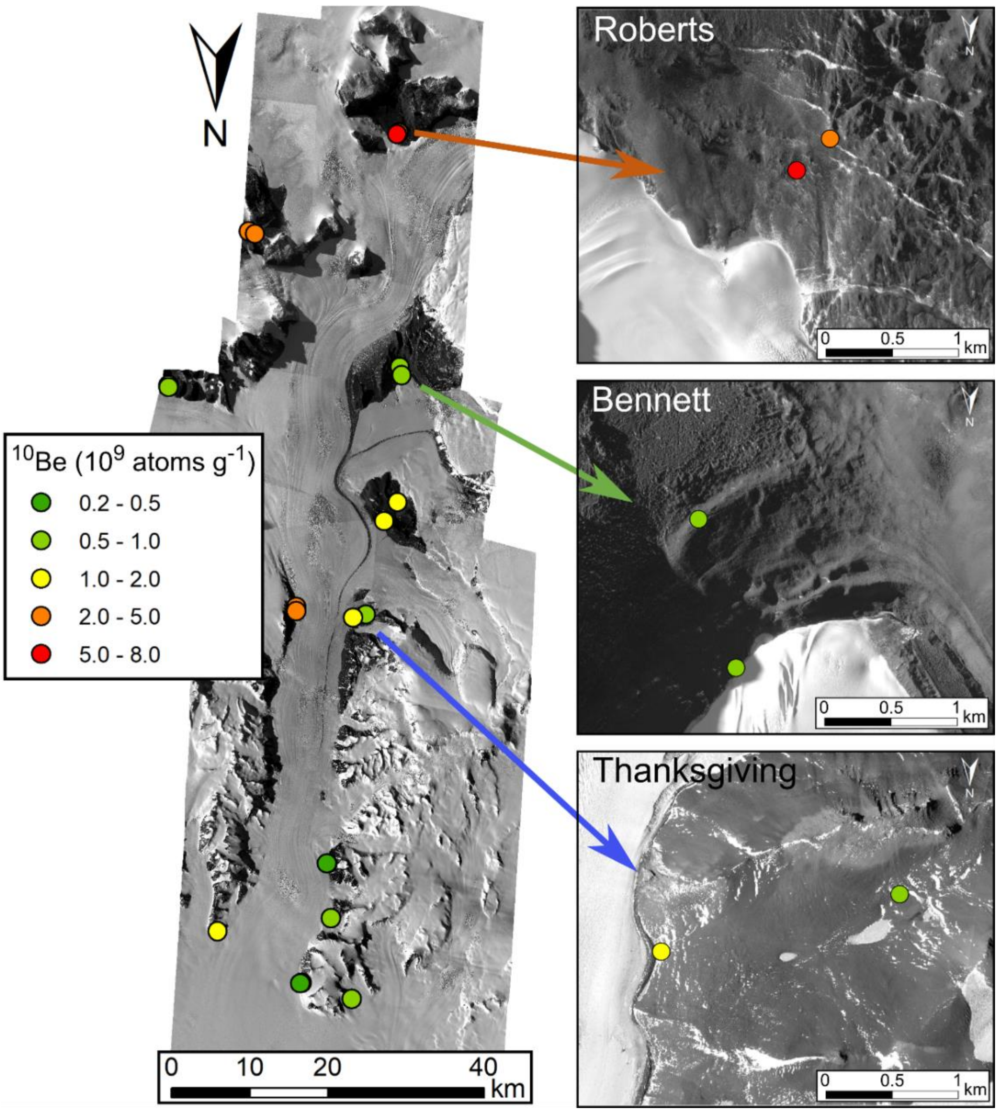

https://doi.org/10.5194/esurf-2020-50
Preprint. Discussion started: 8 July 2020

Earth Surface Dynamics Discussions Open Access EGU

415 **Figure 5:** Concentration of meteoric ^{10}Be with elevation and distance from coast. The solid black lines are linear regressions.
416

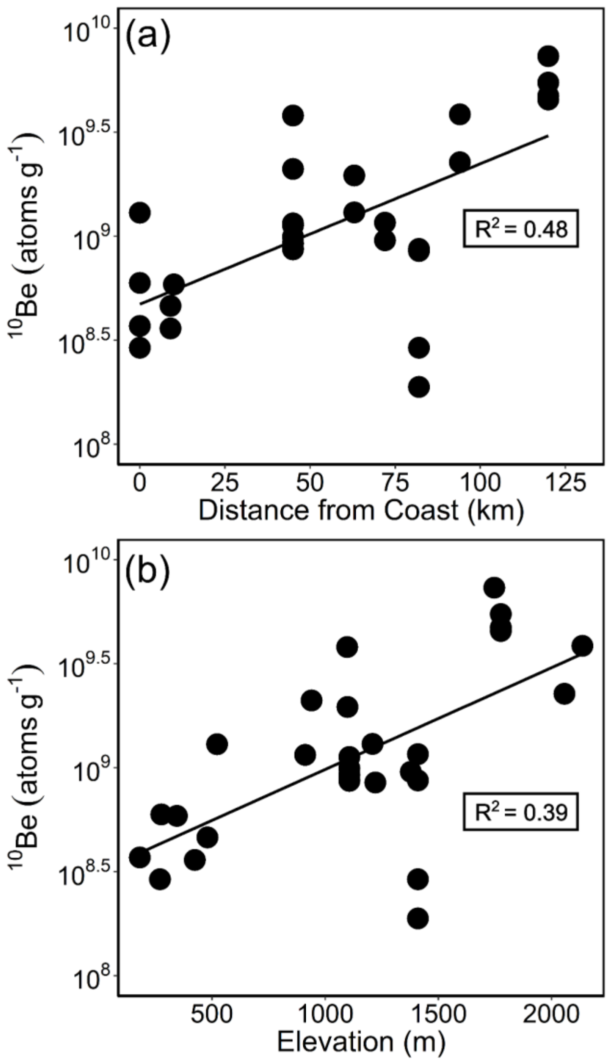

417

https://doi.org/10.5194/esurf-2020-50
Preprint. Discussion started: 8 July 2020

418 **Figure 6:** The grain size composition of soil profiles collected from Roberts Massif (a, orange), Bennett Platform (b, green),
419 and Thanksgiving Valley (c, blue). The soil pits from Bennett Platform and Thanksgiving Valley are also shown with
420 distinct soil horizons.
421

422 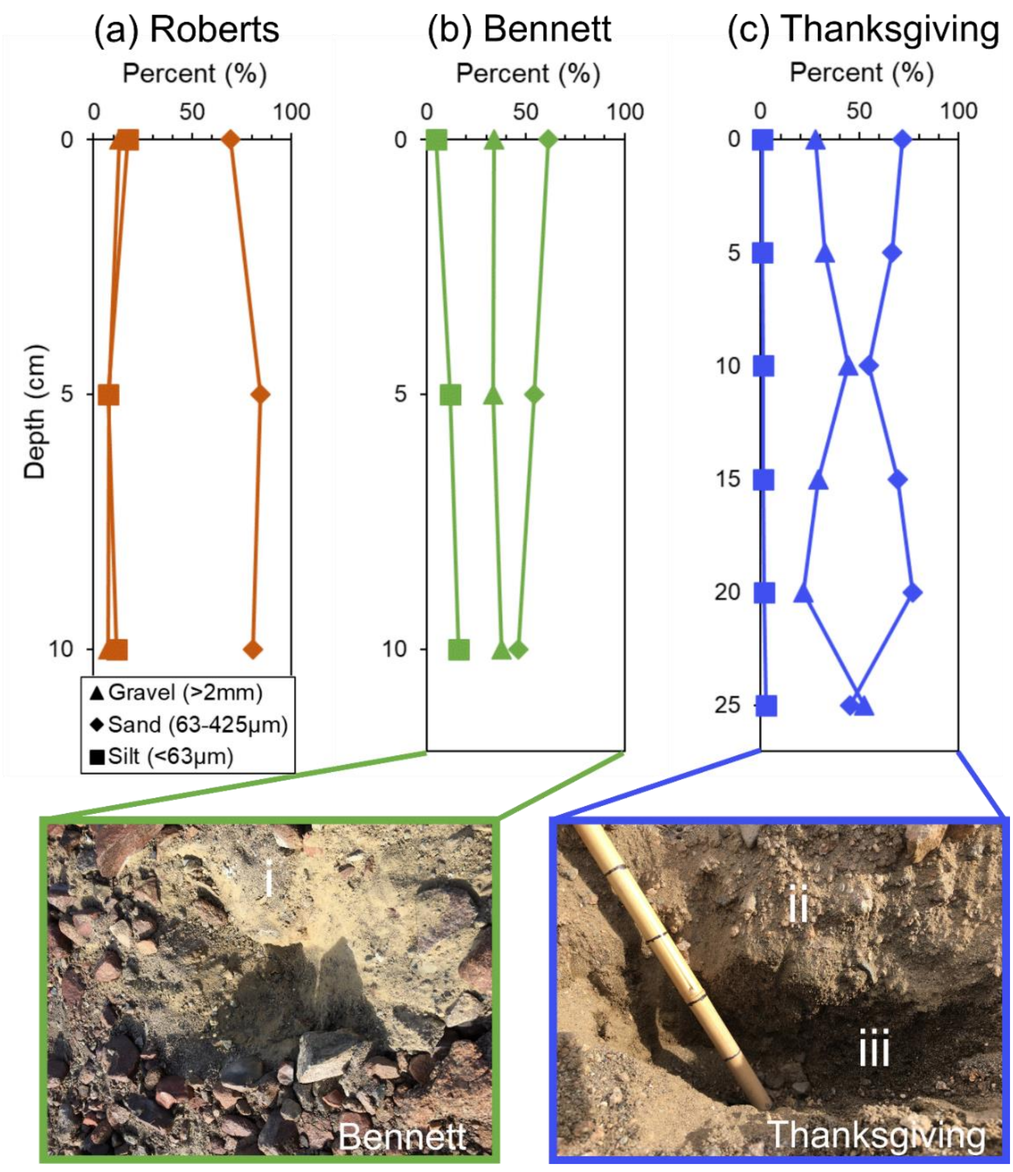

https://doi.org/10.5194/esurf-2020-50
Preprint. Discussion started: 8 July 2020

Figure 7: Soil profiles of meteoric ^{10}Be concentrations for Roberts Massif (orange), Bennett Platform (green), and Thanksgiving Valley (blue) compared to profiles from the Antarctic (Dickinson et al., 2012[*]; Schiller et al., 2009[†]; Valletta et al., 2015[‡]) and Arctic (Bierman et al., 2014[¶]; Ebert et al., 2012[§]) (a). The ^{10}Be concentration profiles were also compared to NO_3^- concentration profiles (b) and a power function was fit to the data (c).

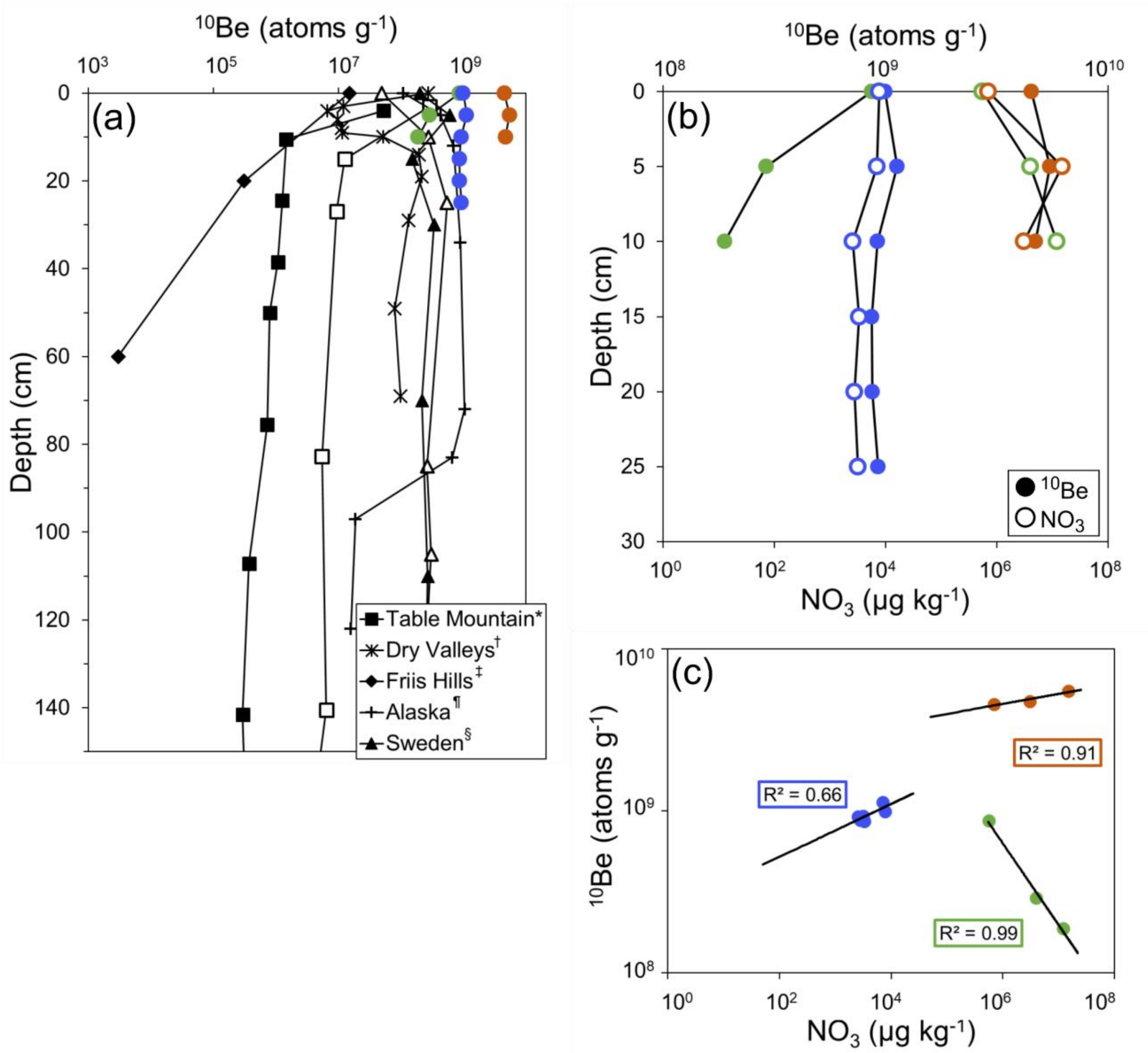

https://doi.org/10.5194/esurf-2020-50
Preprint. Discussion started: 8 July 2020

Earth Surface Dynamics Discussions
Open Access
EGU

Figure 8: Estimated maximum age versus distance from the coast (a) and elevation (b). The blue triangles represent the maximum age estimates using the relationship between NO_3^- and ^{10}Be, black and white triangles represent maximum age estimates using inferred ^{10}Be inventories. Upward facing triangles are samples collected furthest from the glacier, while downward triangles are samples collected closest to the glacier. Sample RM2-8 (Roberts Massif, closest to glacier) is outside the range. Linear regression lines are plotted for the three datasets where the solid line is for the NO_3^- estimate, the dashed line is the inferred estimate for samples furthest from the glacier, and the dotted line is the inferred estimate for samples closest to the glacier. The estimated maximum ages (blue) and inheritance-corrected ages (grey) using the NO_3^- concentrations are overlaid on a map of the Shackleton Glacier region (c).

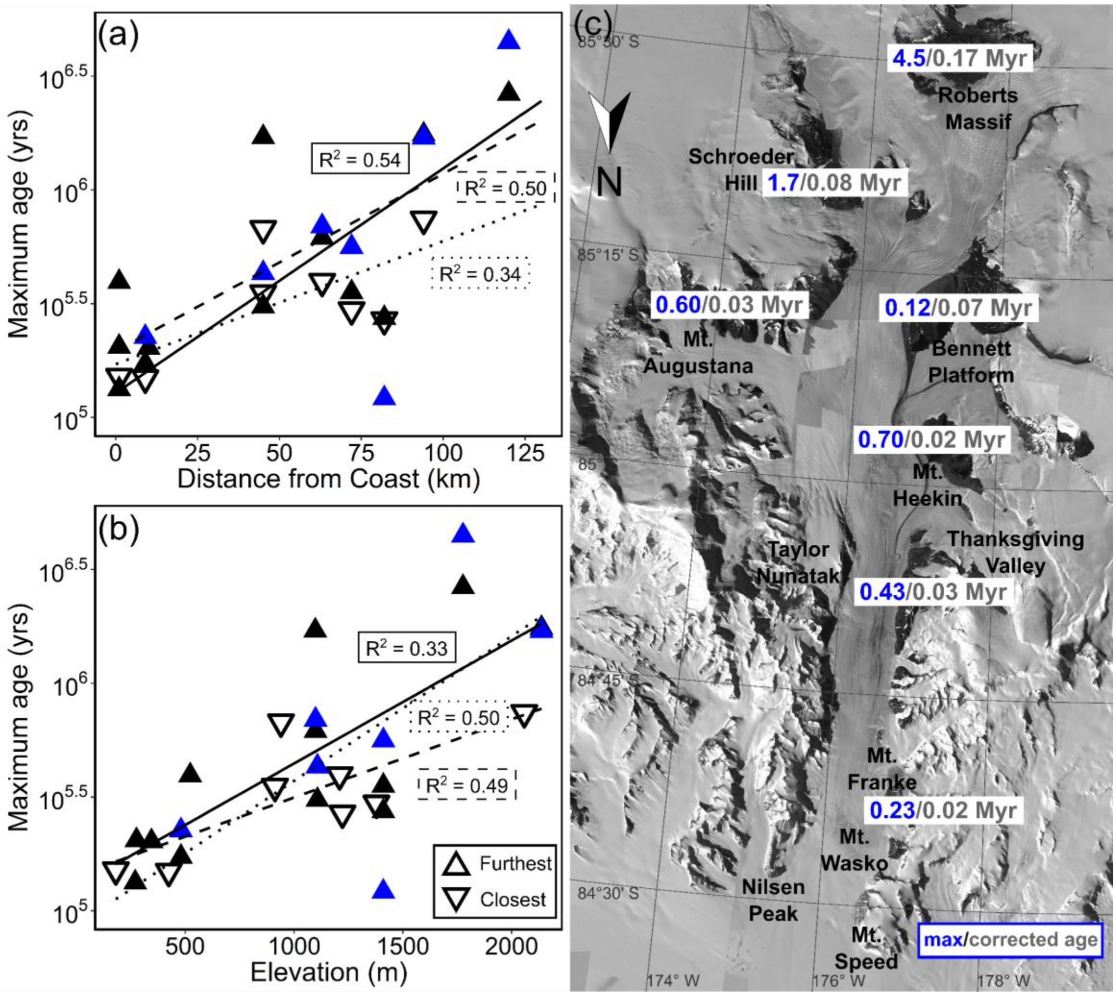

Tables:

Table 1: Geographic data of samples collected from eleven ice-free areas along the Shackleton Glacier. Distance from the coast (aerial) was measured post-collection using ArcMap 10.3 software. Samples of the format "X-1" are samples collected furthest from the glacier in the transect.

Location	Sample name	Latitude	Longitude	Elevation (m)	Distance from coast (km)
Mt. Augustana	AV2-1	-85.1706	-174.1338	1410	72
Mt. Augustana	AV2-8	-85.1676	-174.1393	1378	72
Bennett Platform	BP2-1	-85.2121	-177.3576	1410	82
Bennett Platform	BP2-8	-85.2024	-177.3907	1222	82
Mt. Franke	MF2-1	-84.6236	-176.7353	480	9
Mt. Franke	MF2-4	-84.6237	-176.7252	424	9
Mt. Heekin	MH2-1	-85.0299	-177.2405	1098	63
Mt. Heekin	MH2-8	-85.0528	-177.4099	1209	63
Mt. Speed	MSP2-1	-84.4819	-176.5070	270	0
Mt. Speed	MSP2-4	-84.4811	-176.4864	181	0
Mt. Speed	MSP4-1	-84.4661	-177.1224	276	0
Mt. Wasko	MW4-1	-84.5600	-176.8177	345	10
Nilsen Peak	NP2-5	-84.6227	-176.7501	522	0
Roberts Massif	RM2-1	-85.4879	-177.1844	1776	120
Roberts Massif	RM2-8	-85.4857	-177.1549	1747	120
Schroeder Hill	SH3-2	-85.3597	-175.0693	2137	94
Schroeder Hill	SH3-8	-85.3569	-175.1621	2057	94
Thanksgiving Valley	TGV2-1	-84.9190	-177.0603	1107	45
Thanksgiving Valley	TGV2-8	-84.9145	-176.8860	912	45
Taylor Nunatak	TN3-1	-84.9227	-176.1242	1097	45
Taylor Nunatak	TN3-5	-84.9182	-176.1282	940	45

https://doi.org/10.5194/esurf-2020-50
Preprint. Discussion started: 8 July 2020

Table 2: Concentration of meteoric ^{10}Be in Shackleton Glacier region surface soils and depth profiles from Roberts Massif, Bennett Platform, and Thanksgiving Valley.

Sample name	Sample mass (g)	Mass of ^{9}Be added (µg)*	AMS Cathode Number	Uncorrected ^{10}Be/^{9}Be ratio (10^{-11})**	Uncorrected ^{10}Be/^{9}Be ratio uncertainty (10^{-13})**	Background-corrected ^{10}Be/^{9}Be ratio (10^{-11})***	Background-corrected ^{10}Be/^{9}Be ratio uncertainty (10^{-13})***	^{10}Be concentration (10^{9} atoms g^{-1})	^{10}Be concentration uncertainty (10^{7} atoms g^{-1})
AV2-1	0.499	394.3	151135	2.201	1.143	2.201	1.143	1.162	0.604
AV2-8	0.500	400.2	151137	1.786	1.067	1.785	1.067	0.955	0.571
BP2-1, 0-5	0.499	401.2	151147	1.616	1.055	1.615	1.055	0.868	0.567
BP2-1, 5-10	0.499	399.2	151148	0.353	0.748	0.352	0.748	0.188	0.400
BP2-1, 10-15	0.496	400.2	151149	1.573	1.894	1.573	1.894	0.848	1.021
BP2-8	0.498	400.2	151550	0.542	0.448	0.541	0.448	0.291	0.241
MF2-1	0.505	398.2	151554	3.713	3.444	3.712	3.444	1.956	1.815
MF2-4	0.501	398.2	151555	2.448	1.395	2.447	1.396	1.300	0.741
MH2-1	0.498	399.2	151138	0.864	0.820	0.863	0.820	0.462	0.439
MH2-8	0.499	395.3	151139	0.681	0.847	0.680	0.847	0.360	0.449
MSP2-1	0.499	403.2	151556	0.539	0.464	0.538	0.464	0.291	0.250
MSP2-4	0.502	402.2	151557	0.693	0.673	0.692	0.674	0.370	0.361
MSP4-1	0.499	400.2	151566	1.112	1.117	1.111	1.117	0.596	0.598
MW4-1	0.498	400.2	151564	1.093	0.662	1.092	0.662	0.586	0.356
NP2-5	0.496	402.2	151565	2.391	1.200	2.391	1.200	1.295	0.650
RM2-1, 0-5	0.502	399.2	151558	8.541	4.116	8.541	4.116	4.538	2.187
RM2-1, 5-10	0.499	398.2	151559	8.853	8.411	8.852	8.411	4.721	4.485
RM2-1, 10-15	0.500	400.2	151560	13.70	8.460	13.70	8.460	7.327	4.524
RM2-8	0.498	401.2	151561	10.17	15.27	10.17	15.27	5.475	8.221
SH3-2	0.497	398.2	151551	7.191	3.129	7.190	3.129	3.850	1.675
SH3-8	0.501	398.2	151552	4.270	3.351	4.269	3.351	2.267	1.780
TGV2-1, 0-5	0.498	398.2	151140	1.860	2.431	1.859	2.431	0.993	1.299

https://doi.org/10.5194/esurf-2020-50
Preprint. Discussion started: 8 July 2020

TGV2-1, 5-10	0.500	398.2	151141	1.731	1.589	1.731	1.589	0.921	0.846
TGV2-1, 10-15	0.497	393.3	151142	1.635	1.377	1.634	1.377	0.864	0.728
TGV2-1, 15-20	0.502	399.2	151143	1.645	1.776	1.645	1.777	0.874	0.944
TGV2-1, 20-25	0.498	403.2	151144	1.711	0.852	1.710	0.852	0.925	0.461
TGV2-1, 25-30	0.497	399.2	151145	2.148	2.071	2.147	2.071	1.152	1.112
TGV2-8	0.499	399.2	151146	2.106	2.185	2.105	2.185	1.125	1.168
TN3-1	0.500	401.2	151562	7.092	5.903	7.091	5.903	3.802	3.165
TN3-5	0.500	401.2	151563	3.926	5.694	3.925	5.694	2.105	3.053

*^{9}Be was added through commercial SPEX carrier with a concentration of 1000 μg mL^{-1}.

**Isotopic analysis was conducted at PRIME Laboratory; ratios were normalized against standard 07KNSTD3110 with an assumed ratio of 2850 x 10^{-15} (Nishiizumi et al., 2007). Blank ^{10}Be/^{9}Be ratio values averaged 8.152 ± 1.884 x 10^{-15}.

https://doi.org/10.5194/esurf-2020-50
Preprint. Discussion started: 8 July 2020

Earth Surface Dynamics Discussions
Open Access
EGU

Table 3: Exposure ages calculated from Eq. (1-5) and estimated ages using NO_3^- concentration data.

Location	**Calculated inventory (10^{11} atoms cm^{-2})**	**Calculated inheritance (10^{11} atoms cm^{-2})**	**Calculated max exposure age (10^6 yrs)**	**Calculated exposure age with inheritance (10^6 yrs)**	**Estimated inventory (10^{11} atoms cm^{-2})***	**Estimated inheritance (10^{11} atoms cm^{-2})***	**Estimated max exposure age (10^6 yrs)***	**Estimated exposure age with inheritance (10^6 yrs)***
Augustana	-	-	-	-	0.58	0.55	0.60	0.03
Bennett	0.13	0.06	0.11	0.07	0.14	0.06	0.12	0.07
Franke	-	-	-	-	0.27	0.25	0.23	0.02
Heekin	-	-	-	-	0.65	0.63	0.70	0.02
Roberts	1.47	1.36	4.09	0.14	1.51	1.37	4.54	0.17
Schroeder	-	-	-	-	1.05	0.98	1.66	0.08
Thanksgiving	0.57	0.52	0.54	0.04	0.47	0.43	0.43	0.03

*Estimations derived from power relationship between NO_3^- concentration and meteoric ^{10}Be concentration

https://doi.org/10.5194/esurf-2020-50
Preprint. Discussion started: 8 July 2020

Earth Surface Dynamics Discussions Open Access EGU

Table 4: Estimated exposure ages using relationship between maximum ^{10}Be concentration and inventory in Figure S1 (Bierman et al., 2014).

Sample name	Estimated inventory (10^{11} atoms cm^{-2})	Estimated max exposure age (10^6 yrs)
AV2-1	0.38	0.35
AV2-8	0.33	0.30
BP2-1	0.31	0.27
BP2-8	0.31	0.27
MF2-1	0.21	0.17
MF2-4	0.18	0.15
MH2-1	0.59	0.62
MH2-8	0.42	0.40
MSP2-1	0.16	0.13
MSP2-4	0.18	0.15
MSP4-1	0.24	0.20
MW4-1	0.24	0.20
N2-5	0.42	0.39
RM2-1	1.24	2.65
RM2-8	1.50	>14*
SH3-2	1.07	1.75
SH3-8	0.67	0.74
TGV2-1	0.34	0.31
TGV2-8	0.38	0.35
TN3-1	1.06	1.70
TN3-5	0.62	0.68
*Outside of model range		

https://doi.org/10.5194/esurf-2020-50
Preprint. Discussion started: 8 July 2020

Earth Surface Dynamics Discussions Open Access EGU

References

Ackert, R. P. and Kurz, M. D.: Age and uplift rates of Sirius Group sediments in the Dominion Range, Antarctica, from surface exposure dating and geomorphology, Glob. Planet. Change, 42(1–4), 207–225, doi:10.1016/j.gloplacha.2004.02.001, 2004.

Balco, G.: Contributions and unrealized potential contributions of cosmogenic-nuclide exposure dating to glacier chronology, 1990-2010, Quat. Sci. Rev., 30(1–2), 3–27, doi:10.1016/j.quascirev.2010.11.003, 2011.

Balco, G.: Technical note: A prototype transparent-middle-layer data management and analysis infrastructure for cosmogenic-nuclide exposure dating, Geochronol. Discuss., in review, doi:10.5194/gchron-2020-6, 2020.

Balco, G., Stone, J. O. H., Sliwinski, M. G. and Todd, C.: Features of the glacial history of the Transantarctic Mountains inferred from cosmogenic 26 Al, 10 Be and 21 Ne concentrations in bedrock surfaces, Antarct. Sci., 26(6), 708–723, doi:10.1017/S0954102014000261, 2019.

Balter, A., Bromley, G., Balco, G., Thomas, H. and Jackson, M. S.: A 14.5 million-year record of East Antarctic Ice Sheet fluctuations from the central Transantarctic Mountains, 2 constrained with cosmogenic, Cryosph. Discuss., in review, doi:10.5194/tc-2020-57, 2020.

Barrett, P.: Resolving views on Antarctic Neogene glacial history-The Sirius debate Antarctic climate history View project, Earth Environ. Sci. Trans. R. Soc. Edinburgh, 104(01), 31–53, doi:10.1017/S175569101300008X, 2013.

Barrett, P. J., Adams, C. J., McIntosh, W. C., Swisher, C. C. and Wilson, G. S.: Geochronological evidence supporting Antarctic deglaciation three million years ago, Nature, 359, 816–818, 1992.

Bierman, P. R., Corbett, L. B., Graly, J. A., Neumann, T. A., Lini, A., Crosby, B. T. and Rood, D. H.: Preservation of a Preglacial Landscape Under the Center of the Greenland Ice Sheet, Science (80-.)., 344, 402–405, doi:10.4159/harvard.9780674430501.c21, 2014.

Blunier, T. and Brook, E. J.: Timing of millennial-scale climate change in antarctica and greenland during the last glacial period, Science (80-.)., 291(5501), 109–112, doi:10.1126/science.291.5501.109, 2001.

Bromley, G. R. M., Hall, B. L., Stone, J. O., Conway, H. and Todd, C. E.: Late Cenozoic deposits at Reedy Glacier, Transantarctic Mountains: implications for former thickness of the West Antarctic Ice Sheet, Quat. Sci. Rev., 29(3–4), 384–398, doi:10.1016/j.quascirev.2009.07.001, 2010.

Brook, E. J., Kurz, M. D., Ackert, R. P., Denton, G. H., Brown, E. T., Raisbeck, G. M. and Yiou, F.: Chronology of taylor glacier advances in Arena Valley, Antarctica, using in situ cosmogenic 3He and 10Be, Quat. Res., 39(1), 11–23, doi:10.1006/qres.1993.1002, 1993.

Brook, E. J., Brown, E. T., Kurz, M. D., Ackert, R. P., Raisbeck, G. M. and Yiou, F.: Constraints on age, erosion, and uplift of Neogene glacial deposits in the Transantarctic Mountains determined from in situ cosmogenic 10Be and 26Al, Geology, 23(12), 1063–1066, doi:10.1130/0091-7613(1995)023<1063:coaeau>2.3.co;2, 1995.

Brown, E. T., Edmond, J. M., Raisbeck, G. M., Bourlès, D. L., Yiou, F. and Measures, C. I.: Beryllium isotope geochemistry in tropical river basins, Geochim. Cosmochim. Acta, 56(4), 1607–1624, doi:10.1016/0016-7037(92)90228-B, 1992.

Bruno, L. A., Baur, H., Graf, T., Schlüchter, C., Signer, P. and Wieler, R.: Dating of Sirius Group tillites in the Antarctic Dry Valleys with cosmogenic 3He and 21Ne., 1997.

Claridge, G. G. C. and Campbell, I. B.: Soils of the Shackleton glacier region, Queen Maud Range, Antarctica, New Zeal. J. Sci., 11(2), 171–218, 1968.

Clark, P. U., Dyke, A. S., Shakun, J. D., Carlson, A. E., Clark, J., Wohlfarth, B., Mitrovica, J. X., Hostetler, S. W. and McCabe, A. M.: The Last Glacial Maximum, Science (80-.)., 325, 710–714, doi:10.1126/science.1172873, 2009.

DeConto, R. M. and Pollard, D.: Contribution of Antarctica to past and future sea-level rise, Nature, 531(7596), 591–597, doi:10.1038/nature17145, 2016.

https://doi.org/10.5194/esurf-2020-50
Preprint. Discussion started: 8 July 2020

Earth Surface Dynamics Discussions

Denton, G. H., Sugden, D. E., Marchant, D. R., Hall, B. L. and Wilch, T. I.: East Antarctic Ice Sheet Sensitivity to Pliocene Climatic Change from a Dry Valleys Perspective, Source Geogr. Ann. Ser. A, 75(4), 155–204, 1993.

Dickinson, W. W., Schiller, M., Ditchburn, B. G., Graham, I. J. and Zondervan, A.: Meteoric Be-10 from Sirius Group suggests high elevation McMurdo Dry Valleys permanently frozen since 6 Ma, Earth Planet. Sci. Lett., 355–356, 13–19, doi:10.1016/j.epsl.2012.09.003, 2012.

Dolan, A. M., De Boer, B., Bernales, J., Hill, D. J. and Haywood, A. M.: High climate model dependency of Pliocene Antarctic ice-sheet predictions, Nat. Commun., 9(1), 1–12, doi:10.1038/s41467-018-05179-4, 2018.

Dwyer, G. S. and Chandler, M. A.: Mid-Pliocene sea level and continental ice volume based on coupled benthic Mg/Ca palaeotemperatures and oxygen isotopes, Philos. Trans. R. Soc. A Math. Phys. Eng. Sci., 367(1886), 157–168, doi:10.1098/rsta.2008.0222, 2009.

Ebert, K., Willenbring, J., Norton, K. P., Hall, A. and Hättestrand, C.: Meteoric 10 Be concentrations from saprolite and till in northern Sweden: Implications for glacial erosion and age, , doi:10.1016/j.quageo.2012.05.005, 2012.

Elliot, D. H. and Fanning, C. M.: Detrital zircons from upper Permian and lower Triassic Victoria Group sandstones, Shackleton Glacier region, Antarctica: Evidence for multiple sources along the Gondwana plate margin, Gondwana Res., 13, 259–274, doi:10.1016/j.gr.2007.05.003, 2008.

Frey, M. M., Savarino, J., Morin, S., Erbland, J. and Martins, J. M. F.: Photolysis imprint in the nitrate stable isotope signal in snow and atmosphere of East Antarctica and implications for reactive nitrogen cycling., 2009.

Golledge, N. R. and Levy, R. H.: Geometry and dynamics of an East Antarctic Ice Sheet outlet glacier, under past and present climates, J. Geophys. Res., 116(F3), F03025, doi:10.1029/2011JF002028, 2011.

Golledge, N. R., Levy, R. H., McKay, R. M., Fogwill, C. J., White, D. A., Graham, A. G. C., Smith, J. A., Hillenbrand, C. D., Licht, K. J., Denton, G. H., Ackert, R. P., Maas, S. M. and Hall, B. L.: Glaciology and geological signature of the Last Glacial Maximum Antarctic ice sheet, Quat. Sci. Rev., 78, 225–247, doi:10.1016/j.quascirev.2013.08.011, 2013.

Graham, I., Ditchburn, R. G., Claridge, G. G. G., Whitehead, N. E., Zondervan, A. and Sheppard, D. S.: Dating Antarctic soils using atmospheric derived 10Be and nitrate, R. Soc. New Zeal. Bull., 35, 429–436, 2002.

Graly, J. A., Bierman, P. R., Reusser, L. J. and Pavich, M. J.: Meteoric 10Be in soil profiles - A global meta-analysis, Geochim. Cosmochim. Acta, 74, 6814–6829, doi:10.1016/j.gca.2010.08.036, 2010.

Graly, J. A., Licht, K. J., Druschel, G. K. and Kaplan, M. R.: Polar desert chronologies through quantitative measurements of salt accumulation, Geology, 46(4), 351–354, doi:10.1130/G39650.1, 2018.

Hambrey, M. J., Webb, P. N., Harwood, D. M. and Krissek, L. A.: Neogene glacial record from the Sirius Group of the Shackleton Glacier region, central Transantarctic Mountains, Antarctica, GSA Bull., 115(8), 994–1015, doi:10.1130/B25183.1, 2003.

Higgins, S. M., Hendy, C. H. and Denton, G. H.: Geochronology of Bonney Drift, Taylor Valley, Antarctica: Evidence for interglacial expansions of Taylor Glacier, Geogr. Ann. Ser. A Phys. Geogr., 82(2–3), 391–409, doi:10.1111/j.0435-3676.2000.00130.x, 2000.

Huybrechts, P.: Glaciological Modelling of the Late Cenozoic East Antarctic Ice Sheet: Stability or Dynamism?, Geogr. Ann. Ser. A, Phys. Geogr., 75(4), 221–238, doi:10.1080/04353676.1993.11880395, 1993.

Ivy-Ochs, S., Schluchter, C., Kubik, P. W., Dittrich-Hannen, B. and Beer, J.: Minimum 10Be exposure ages of early Pliocene for the Table Mountain plateau and the Sirius Group at Mount Fleming, Dry Valleys, Antarctica, Geology, 23(11), 1007–1010, 1995.

Jackson, M. S., Hall, B. L. and Denton, G. H.: Asynchronous behavior of the Antarctic Ice Sheet and local glaciers during and since Termination 1, Salmon Valley, Antarctica, Earth Planet. Sci. Lett., 482, 396–406, doi:10.1016/j.epsl.2017.11.038, 2018.

Jones, R. S., Mackintosh, A. N., Norton, K. P., Golledge, N. R., Fogwill, C. J., Kubik, P. W., Christl, M. and

Greenwood, S. L.: Rapid Holocene thinning of an East Antarctic outlet glacier driven by marine ice sheet instability, Nat. Commun., 6(8910), 9910, doi:10.1038/ncomms9910, 2015.

Kaplan, M. R., Licht, K. J., Winckler, G., Schaefer, J. M., Bader, N., Mathieson, C., Roberts, M., Kassab, C. M., Schwartz, R. and Graly, J. A.: Middle to Late Pleistocene stability of the central East Antarctic Ice Sheet at the head of Law Glacier, Geology, 45(11), 963–966, doi:10.1130/G39189.1, 2017.

Lewis, A. R., Marchant, D. R., Ashworth, A. C., Hedenäs, L., Hemming, S. R., Johnson, J. V., Leng, M. J., Machlus, M. L., Newton, A. E., Raine, J. I., Willenbring, J. K., Williams, M. and Wolfe, A. P.: Mid-Miocene cooling and the extinction of tundra in continental Antarctica, Proc. Natl. Acad. Sci. U. S. A., 105(31), 10676–10680, doi:10.1073/pnas.0802501105, 2008.

Lyons, W. B., Deuerling, K., Welch, K. A., Welch, S. A., Michalski, G., Walters, W. W., Nielsen, U., Wall, D. H., Hogg, I. and Adams, B. J.: The Soil Geochemistry in the Beardmore Glacier Region, Antarctica: Implications for Terrestrial Ecosystem History, Sci. Rep., 6, 26189, doi:10.1038/srep26189, 2016.

Mackintosh, A. N., Verleyen, E., O'Brien, P. E., White, D. A., Jones, R. S., McKay, R., Dunbar, R., Gore, D. B., Fink, D., Post, A. L., Miura, H., Leventer, A., Goodwin, I., Hodgson, D. A., Lilly, K., Crosta, X., Golledge, N. R., Wagner, B., Berg, S., van Ommen, T., Zwartz, D., Roberts, S. J., Vyverman, W. and Masse, G.: Retreat history of the East Antarctic Ice Sheet since the Last Glacial Maximum, Quat. Sci. Rev., 100, 10–30, doi:10.1016/j.quascirev.2013.07.024, 2014.

Marchant, D. R., Denton, G. H., Bockheim, J. G., Wilson, S. C. and Kerr, A. R.: Quaternary changes in level of the upper Taylor Glacier, Antarctica: implications for paleoclimate and East Antarctic Ice Sheet dynamics, Boreas, 23(1), 29–43, doi:10.1111/j.1502-3885.1994.tb00583.x, 1994.

Marchant, D. R., Denton, G. H., Swisher, C. C. and Potter, N.: Late Cenozoic Antarctic paleoclimate reconstructed from volcanic ashes in the Dry Valleys region of southern Victoria Land, Geol. Soc. Am. Bull., 108(2), 181–194, doi:https://doi.org/10.1130/0016-7606(1996)108%3C0181:LCAPRF%3E2.3.CO;2, 1996.

Margerison, H. R., Phillips, W. M., Stuart, F. M. and Sugden, D. E.: Cosmogenic 3He concentrations in ancient flood deposits from the Coombs Hills, northern Dry Valleys, East Antarctica: interpreting exposure ages and erosion rates, Earth Planet. Sci. Lett., 230(1–2), 163–175, doi:10.1016/J.EPSL.2004.11.007, 2005.

McHargue, L. R. and Damon, P. E.: The global beryllium 10 cycle, Rev. Geophys., 29(2), 141–158, doi:10.1029/91RG00072, 1991.

McKay, R., Browne, G., Carter, L., Cowan, E., Dunbar, G., Krissek, L., Naish, T., Powell, R., Reed, J., Talarico, F. and Wilch, T.: The stratigraphic signature of the late Cenozoic Antarctic Ice Sheets in the Ross Embayment, Bull. Geol. Soc. Am., 121(11–12), 1537–1561, doi:10.1130/B26540.1, 2009.

Michalski, G., Bockheim, J. G., Kendall, C. and Thiemens, M.: Isotopic composition of Antarctic Dry Valley nitrate: Implications for NOy sources and cycling in Antarctica, Geophys. Res. Lett., 32(13), 1–4, doi:10.1029/2004GL022121, 2005.

Morgan, D., Putkonen, J., Balco, G. and Stone, J.: Quantifying regolith erosion rates with cosmogenic nuclides 10 Be and 26 Al in the McMurdo Dry Valleys, Antarctica, J. Geophys. Res., 115, F03037, doi:10.1029/2009JF001443, 2010.

Naish, T., Powell, R., Levy, R., Wilson, G., Scherer, R., Talarico, F., Krissek, L., Niessen, F., Pompilio, M., Wilson, T., Carter, L., DeConto, R., Huybers, P., McKay, R., Pollard, D., Ross, J., Winter, D., Barrett, P., Browne, G., Cody, R., Cowan, E., Crampton, J., Dunbar, G., Dunbar, N., Florindo, F., Gebhardt, C., Graham, I., Hannah, M., Hansaraj, D., Harwood, D., Helling, D., Henrys, S., Hinnov, L., Kuhn, G., Kyle, P., Läufer, A., Maffioli, P., Magens, D., Mandernack, K., McIntosh, W., Millan, C., Morin, R., Ohneiser, C., Paulsen, T., Persico, D., Raine, I., Reed, J., Riesselman, C., Sagnotti, L., Schmitt, D., Sjunneskog, C., Strong, P., Taviani, M., Vogel, S., Wilch, T. and Williams, T.: Obliquity-paced Pliocene West Antarctic ice sheet oscillations, Nature, 458(7236), 322–328, doi:10.1038/nature07867, 2009.

Nishiizumi, K., Imamura, M., Caffee, M. W., Southon, J. R., Finkel, R. C. and McAninch, J.: Absolute calibration of 10Be AMS standards, Nucl. Instruments Methods Phys. Res. B, 258, 403–413, doi:10.1016/j.nimb.2007.01.297,

https://doi.org/10.5194/esurf-2020-50
Preprint. Discussion started: 8 July 2020

2007.

Paulsen, T. S., Encarnación, J. and Grunow, A. M.: Structure and timing of transpressional deformation in the Shackleton Glacier area, Ross orogen, Antarctica, J. Geol. Soc. London., 161(6), 1027–1038, doi:10.1144/0016-764903-040, 2004.

Pavich, M. J., Brown, L., Klein, J. and Middleton, R.: 10Be accumulation in a soil chronosequence, Earth Planet. Sci. Lett., 68, 198–204, doi:10.1016/0012-821X(84)90151-1, 1984.

Pavich, M. J., Brown, L., Harden, J., Klein, J. and Middleton, R.: 10Be distribution in soils from Merced River terraces, California, Geochim. Cosmochim. Acta, 50, 1727–1735, doi:10.1016/0016-7037(86)90134-1, 1986.

Pollard, D. and DeConto, R. M.: Modelling West Antarctic ice sheet growth and collapse through the past five million years, Nature, 458(7236), 329–332, doi:10.1038/nature07809, 2009.

Scherer, R. P., Aldahan, A., Tulaczyk, S., Possnert, G., Engelhardt, H. and Kamb, B.: Pleistocene collapse of the West Antarctic ice sheet, Science (80-.)., 281(5373), 82–85, doi:10.1126/science.281.5373.82, 1998.

Scherer, R. P., DeConto, R. M., Pollard, D. and Alley, R. B.: Windblown Pliocene diatoms and East Antarctic Ice Sheet retreat, Nat. Commun., 7(1), 1–9, doi:10.1038/ncomms12957, 2016.

Schiller, M., Dickinson, W., Ditchburn, R. G., Graham, I. J. and Zondervan, A.: Atmospheric 10 Be in an Antarctic soil: Implications for climate change, J. Geophys. Res., 114(F1), 1–8, doi:10.1029/2008jf001052, 2009.

Shakun, J. D., Corbett, L. B., Bierman, P. R., Underwood, K., Rizzo, D. M., Zimmerman, S. R., Caffee, M. W., Naish, T., Golledge, N. R. and Hay, C. C.: Minimal East Antarctic Ice Sheet retreat onto land during the past eight million years, Nature, 558(7709), 284–287, doi:10.1038/s41586-018-0155-6, 2018.

Spector, P., Stone, J., Cowdery, S. G., Hall, B., Conway, H. and Bromley, G.: Rapid early-Holocene deglaciation in the Ross Sea, Antarctica, Geophys. Res. Lett., 44(15), 7817–7825, doi:10.1002/2017GL074216, 2017.

Steig, E., Stuiver, M. and Polissar, P.: Cosmogenic isotope concentrations at Taylor Dome, Antarctica, Antarct. J. United States, 30, 95–97, 1995.

Stone, J.: A rapid fusion method for separation of beryllium-10 from soils and silicates, Geochim. Cosmochim. Acta, 62(3), 555–561, doi:10.1016/S0016-7037(97)00340-2, 1998.

Strasky, S., Di Nicola, L., Baroni, C., Salvatore, M. C., Baur, H., Kubik, P. W., Schlüchter, C. and Wieler, R.: Surface exposure ages imply multiple low-amplitude Pleistocene variations in East Antarctic Ice Sheet, Ricker Hills, Victoria Land, Antarct. Sci., 21(1), 59–69, doi:10.1017/S0954102008001478, 2009.

Stroeven, A. P., Prentice, M. L. and Kleman, J.: On marine microfossil transport and pathways in Antarctica during the late Neogene: Evidence from the Sirius Group at Mount Fleming, Geology, 24(8), 727–730, doi:10.1130/0091-7613(1996)024<0727:ommtap>2.3.co;2, 1996.

Sugden, D. E.: The East Antarctic Ice Sheet: Unstable Ice or Unstable Ideas?, Trans. Inst. Br. Geogr., 21(3), 443, doi:10.2307/622590, 1996.

Sugden, D. E., Marchant, D. R. and Denton, G. H.: The case for a stable East Antarctic ice sheet, Geogr. Ann. Ser. A, 75(4), 151–351, 1993.

Sugden, D. E., Marchant, D. R., Potter, N., Souchez, R. A., Denton, G. H., Swisher, C. C. and Tison, J. L.: Preservation of Miocene glacier ice in East Antarctica, Nature, 376(6539), 412–414, doi:10.1038/376412a0, 1995.

Summerfield, M. A., Stuart, F. M., Cockburn, H. A. P., Sugden, D. E., Denton, G. H., Dunai, T. and Marchant, D. R.: Long-term rates of denudation in the Dry Valleys, Transantarctic Mountains, southern Victoria Land, Antarctica based on in-situ-produced cosmogenic 21Ne, Geomorphology, 27(1–2), 113–129, doi:10.1016/S0169-555X(98)00093-2, 1999.

Valletta, R. D., Willenbring, J. K., Lewis, A. R., Ashworth, A. C. and Caffee, M.: Extreme decay of meteoric beryllium-10 as a proxy for persistent aridity, Sci. Rep., 5, 17813, doi:10.1038/srep17813, 2015.

Webb, P. N. and Harwood, D. M.: Late Cenozoic glacial history of the Ross embayment, Antarctica, Quat. Sci. Rev., 10(2–3), 215–223, doi:10.1016/0277-3791(91)90020-U, 1991.

Webb, P. N., Harwood, D. M., McKelvey, B. C., Mercer, J. H. and Stott, L. D.: Cenozoic marine sedimentation and ice-volume variation on the East Antarctic craton, Geology, 12(5), 287–291, doi:10.1130/0091-7613(1984)12<287:cmsaiv>2.0.co;2, 1984.

Webb, P. N., Harwood, D. M., Mabin, M. G. C. and McKelvey, B. C.: A marine and terrestrial Sirius Group succession, middle Beardmore Glacier-Queen Alexandra Range, Transantarctic Mountains, Antarctica, Mar. Micropaleontol., 27(1–4), 273–297, doi:10.1016/0377-8398(95)00066-6, 1996.

Welch, K. A., Lyons, W. B., Whisner, C., Gardner, C. B., Gooseff, M. N., Mcknight, D. M. and Priscu, J. C.: Spatial variations in the geochemistry of glacial meltwater streams in the Taylor Valley, Antarctica, Antarct. Sci., 22(6), 662–672, doi:10.1017/S0954102010000702, 2010.

Willenbring, J. K. and von Blanckenburg, F.: Meteoric cosmogenic Beryllium-10 adsorbed to river sediment and soil: Applications for Earth-surface dynamics, Earth-Science Rev., 98(1–2), 105–122, doi:10.1016/j.earscirev.2009.10.008, 2010.

Wilson, G. S.: The neogene east antarctic ice sheet: A dynamic or stable feature?, Quat. Sci. Rev., 14(2), 101–123, doi:10.1016/0277-3791(95)00002-7, 1995.

You, C. F., Lee, T. and Li, Y. H.: The partition of Be between soil and water, Chem. Geol., 77(2), 105–118, doi:10.1016/0009-2541(89)90136-8, 1989.